Article

The *In Vitro*, *Ex Vivo*, and *In Vivo* Effect of Polymer Hydrophobicity on Charge-Reversible Vectors for Self-Amplifying RNA

Pratik Gurnani, Anna K. Blakney, Roberto Terracciano, Joshua E. Petch, Andrew J. Blok, Clément R. Bouton, Paul F. McKay, Robin J. Shattock,* and Cameron Alexander*

Read Online

ACCESS | Metrics & More | Article Recommendations | Supporting Information

ABSTRACT: RNA technology has the potential to revolutionize vaccination. However, the lack of clear structure−property relationships in relevant biological models mean there is no clear consensus on the chemical motifs necessary to improve RNA delivery. In this work, we describe the synthesis of a series of copolymers based on the self-hydrolyzing charge-reversible poly-cation poly(dimethylaminoethyl acrylate) (pDMAEA), varying the lipophilicity of the additional co-monomers. All copolymers formed stable polyplexes, showing efficient complexation with model nucleic acids from nitrogen/phosphate (N/P) ratios of N/P = 5, with more hydrophobic complexes exhibiting slower charge reversal and disassembly compared to hydrophilic analogues. The more hydrophobic copolymers outperformed hydrophilic versions, homopolymer controls and the reference standard polymer (polyethylenimine), in transfection assays on 2D cell monolayers, albeit with significantly higher toxicities. Similarly, hydrophobic derivatives displayed up to a 4-fold higher efficacy in terms of the numbers of cells expressing green fluorescent protein (GFP+) cells in *ex vivo* human skin (10%) compared to free RNA (2%), attributed to transfection enrichment in epithelial cells. In contrast, in a mouse model, we observed the reverse trend in terms of RNA transfection, with no observable protein production in more hydrophobic analogues, whereas hydrophilic copolymers induced the highest transfection *in vivo*. Overall, our results suggest an important relationship between the vector lipophilicity and RNA transfection in vaccine settings, with polymer biocompatibility potentially a key parameter in effective *in vivo* protein production.
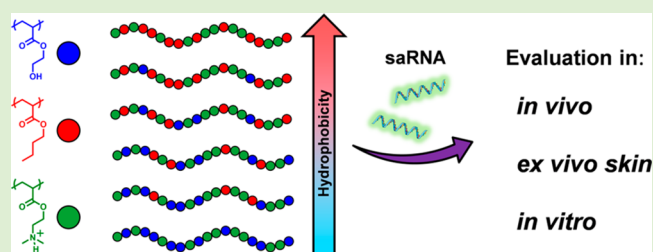
INTRODUCTION

Since the advent of *in vitro* transcription, mRNA (mRNA) therapeutics have evolved into a flexible platform, capable of artificially introducing or replacing specific proteins for vaccination and therapeutic applications.[1,2] The nonintegrating nature of mRNA means that this technology can be easily inserted into current clinical practice, without the long-term safety risks posed with genome altering DNA alternatives.[3−5] As such, several mRNA therapies have undergone, or are currently undergoing clinical trials,[6−8] while their manufacturability is currently under investigation.[9,10]

The activity of RNA therapeutics relies on the efficient delivery of the nucleic acid to the cytosol of the cells at the target site, where it is translated into the active protein. However, naked mRNA suffers from quick pharmacokinetic clearance, poor cellular association and facile degradation, significantly reducing the cytosolic dose and thus its therapeutic activity.[11] Given these drawbacks, numerous nonviral delivery strategies such as liposomes[12,13] and cationic polymers[14−19] which protect, improve pharmacokinetics and aid cytosolic delivery of RNA, have been developed. Strategies exploiting polycations operate by condensing the nucleic acid through electrostatic complexation, forming 100−

200 nm polyelectrolyte nanoparticles termed polyplexes that facilitate translocation of the genetic material into the cell. Most nonviral cationic vectors are designed to complex strongly to nucleic acids to afford protection in transit through the body; however for translation, RNA must also be released from the vector and interact with the cellular protein machinery. Vectors can achieve this release process either by introducing chemistries that break the polycationic chain in response to endogenous stimuli (GSH, ROS, pH, enzymes)[20] or through self-immolative charge alteration, which terminates the electrostatic attraction between a vector and nucleic acid.[21] Although many of the above endogenous stimuli can be useful for delivery in specific disease states, self-immolative pathways for charge reversal may offer a route for mRNA release in the absence of any specific stimuli.

At present, there are few examples of gene delivery using self-immolative charge altering vectors. Notable examples include enhanced mRNA delivery utilizing an oligo-(carbonate-$\beta-\alpha$-amino ester), which rapidly degrades into a neutral diketopiperazine through an ester–amide cyclization reaction, releasing the mRNA.[22] Another key example is the self-catalyzed hydrolysis of poly(dimethylaminoethyl) acrylate (pDMAEA), which degrades from a polycation into poly-anionic poly(acrylic acid) (pAA) in the presence of water releasing dimethylaminoethanol (DMAE).[23−31] From a gene delivery perspective, this delivery system will efficiently condense nucleic acids in their positively charged state and then hydrolyze, charge invert, repel, and release the genetic cargo using a single material. Systems based on the charge-reversing nature of pDMAEA have already been utilized to deliver siRNA[29,31,32] and pDNA;[25] however, no studies have yet examined its potential for mRNA delivery.

It has recently been reported that the introduction of hydrophilic co-monomers, such as poly(dimethylaminoethyl) hydroxymethacrylate,[33] or the spacing of DMAEA units within the chain with nonhydrolyzing DMAEMA can vary the rate and final degree of hydrolysis.[29] Furthermore, to date, most previous examples show a pH-independent hydrolysis mechanism, with few reports showing this can be overcome by hindering the interaction with hydroxide ions.[34] This was achieved by incorporating anionic moieties along the chain; however, such systems would not be beneficial for gene delivery, as they are not net positively charged. Accordingly, we report here a systematic mechanistic study utilizing a library of pDMAEA copolymers, varying the co-monomer lipophilicity to study (a) the effect on hydrolysis rate, (b) if this effects the pH-independent mechanism, and (c) the implications of the co-monomer and charge reversal on mRNA delivery from the perspective of vaccination.

We designed and synthesized a series of pDMAEA copolymers containing varying degrees of a hydrophobic co-monomer, butyl acrylate (BA), and a hydrophilic co-monomer, 2-hydroxyethyl acrylate (HEA), as well as pDMAEA and pDMAEMA (nonhydrolyzing) controls. Hydrolysis was monitored at pH 5.5, 7.4, and 10.1 over 5 days using ¹H NMR spectroscopy. All copolymers were formulated into polyplexes with model nucleic acids, and the particle sizes and zeta-potentials were monitored over 7 days, as the polymers charge inverted. Finally, we evaluated the potential for the vectors to deliver mRNA in a vaccine setting, utilizing a 2D cell culture, in *ex vivo* skin explants and a murine *in vivo* model.

■ MATERIALS AND METHODS

Materials. 2-Hydroxyethyl acrylate (HEA, 96%), butyl acrylate (BA, > 99%), 2-(dimethylamino)ethyl acrylate (DMAEA, > 98%), and 2-(dimethylamino)ethyl methacrylate (DMAEMA, 98%) were obtained from Sigma-Aldrich and the inhibitor removed by passing the monomers through a column of aluminum oxide. Deuterium oxide (99.9% D atom), DMSO-d_6 (99.5% D atom), sodium deuteroxide (40 wt %, 99.5% D atom) and deuterium chloride (35 wt %, 99% D atom) were obtained from Sigma-Aldrich and used for ¹H NMR spectroscopy. Thermal initiators 4,4′-azobis(4-cyanovaleric acid) (ACVA, > 98%) and 1,1′-azobis(1-cyclohexanecarbonitrile) (VA-088, 98%) were purchased from Sigma-Aldrich and used as-received. Reversible addition–fragmentation chain-transfer (RAFT) agents, (4-cyano pentanoic acid)yl ethyl trithiocarbonate (CEPTC), and 2-((butylthio)-carbonothioyl) thio propanoic acid (PABTC) were synthesized as previously reported.[35,36] Ultrapure calf thymus DNA (~2000 bp) was purchased from ThermoFisher Scientific, and

fLuc pDNA (7047 bp), fLuc VEEV saRNA (9382 nt), and eGFP VEEV saRNA (8449 nt) were prepared as described below. Defibrinated sheep blood was purchased from Oxoid, UK. Solvents and other reagents were acquired from commercial sources and used as-received unless stated otherwise.

Methods. *Instrumentation and Analysis. NMR Spectroscopy.* ¹H and ¹³C NMR spectra were recorded on a Bruker DPX-400 spectrometer using deuterated solvent (Materials).

Size Exclusion Chromatography. SEC analysis was performed using a Polymer Laboratories PL-50 instrument fitted with a differential refractive index detector. The system was equipped with 2× PLgel Mixed D columns (300 × 7.5 mm) and a PLgel 5 μm guard column. The eluent used was 0.1% LiBr in dimethylformamide (DMF). Samples were eluted at 1 mL min⁻¹ with the column oven heating to 50 °C. PMMA standards (Agilent EasyVials) were used for conventional calibration between 500−955550 g mol⁻¹. Experimental molar mass ($M_{n,SEC}$) and dispersity (Đ) values of synthesized polymers were determined by using Cirrus GPC software.

Theoretical Molar Mass Calculation. Calculation of the theoretical number-average molar mass ($M_{n,th}$) is shown in the following:

$$M_{n,th} = \frac{[M]_0 p M_M}{[CTA]_0} + M_{CTA} \qquad (1)$$

where $[M]_0$ and $[CTA]_0$ are the initial concentrations (in mol dm⁻³) of the monomer and chain transfer agent, respectively; p is the monomer conversion as determined by ¹H NMR spectroscopy; and M_M and M_{CTA} are the molar masses (g mol⁻¹) of the monomer and chain transfer agent, respectively.

Polymer Synthesis and Characterization. Polymer Synthesis. Polymers were synthesized using the following procedure, utilizing the conditions described in Table S1. RAFT agent (either PABTC or CEPTC), monomer (DMAEA, HEA and BEA in the appropriate ratios), and ACVA were dissolved in 1,4-dioxane. The polymerization vessel was sealed with a septum, and purged with nitrogen for 20 min. The vessel was immersed in an oil bath preheated to 70 °C until the polymerization reached 80−90% monomer conversion as determined by ¹H NMR spectroscopy. Once complete, the polymerization solution was removed from the oil bath, cooled to room temperature, and exposed to oxygen to quench the polymerization. Polymers were purified by precipitation twice in hexane or diethyl ether. The precipitated polymer was dissolved in dichloromethane (DCM), with DCM removed *in vacuo*.

NMR Hydrolysis Assays. Hydrolysis studies to evaluate the kinetics of charge reversal were performed by ¹H NMR spectroscopy. Studies were performed at pH 5.5, 7.4, and 10.1 using acetate, 4-(2-hydroxyethyl)-1-piperazineethanesulfonic acid (HEPES), and carbonate buffers in D₂O, respectively. Buffers were adjusted using NaOD or DCl. P1−P8 (20 mg) were dissolved in each buffer (0.6 mL). Notably, as we prepared solutions with D₂O, a correction factor (pD = pH + 0.41) was applied to account for the difference in acidity between H₂O and D₂O. A crystal of 1,3,5-trioxane was added to the tube as an external reference. ¹H NMR spectra were recorded at 24 h intervals for 5 days. Hydrolysis percentages were calculated based on the integrals at 3.7 (OCH₂ on DMAE residues) and 4.2 ppm (OCH₂ on pDMAEA residues). In some cases where peaks were overlapping, the proton resonances arising from the CH₃ in butyl acrylate at 0.8 ppm were integrated and back-calculated based on the target monomer composition. Furthermore, the hydrophobic derivatives were not fully soluble throughout the study; hence, the DMAE signals at 3.7 ppm were integrated against the 1,3,5-trioxane signals, and at the end of the study, DCl was added to fully solubilize the polymer to calculate the % hydrolysis for each time point.

pH Titration. pH titrations were carried out as previously described.[16] Briefly, 1 mg of polymer (P1−P8 and polyethylenimine (PEI)) was dissolved in 30 mL of NaCl (0.1 M), and the pH was adjusted to 3 through the addition of HCl (0.1 M). The polymer solution was titrated with NaOH (0.1 M), and the pH value of solution was measured until a pH of 5 was achieved.

Nucleic Acid Synthesis. RNA In Vitro Transcription and Purification. saRNA was prepared as previously described.[16] Briefly, self-amplifying RNA encoding the replicase derived from the Venezuelan Equine Encephalitis Virus (VEEV) and either firefly luciferase (fLuc) or enhanced green fluorescent protein (eGFP) was produced using *in vitro* transcription. pDNA was transformed into *Escherichia coli*, cultured in 100 mL of lysogeny broth (LB) with 100 μg/mL carbenicillin (Sigma-Aldrich, UK), and isolated using a Plasmid Plus MaxiPrep kit (QIAGEN, UK). The concentration and purity of pDNA was measured on a NanoDrop One (ThermoFisher, UK) and subsequently linearized using MluI for 3 h at 37 °C. For *in vitro* transfections, capped RNA was synthesized using 1 μg of a linearized DNA template in a mMessage mMachine (Ambion, UK) and purified using a MEGAClear column (Ambion, UK) according to the manufacturer's protocol. RNA for *ex vivo* experiments was prepared as previously described.[37] Uncapped RNA transcripts were synthesized using 1 μg of linearized DNA in a MEGAScript reaction (Ambion, UK) according to the manufacturer's protocol. Transcripts were then purified by overnight LiCl precipitation at −20°C, pelleted by centrifugation at 14000 rpm for 20 min at 4 °C, washed 1× with 70% EtOH, centrifuged for 14000 rpm for 5 min at 4°C, and then resuspended in UltraPure H_2O (Ambion, UK). Purified transcripts were then capped using a ScriptCap Cap 1 capping system kit (CellScript, Madison, WI, USA) according to the manufacturer's protocol. Capped transcripts were then purified by LiCl precipitation as detailed above, resuspended in UltraPure H_2O, and stored at −80°C until further use.

Polyplex Formulation. Polymer Nucleic Acid Complexation. Stock solutions of the polymer and nucleic acid were prepared at double the concentration required in the polyplexes in the HEPES buffer (20 mM, pH 7.4) and 5 wt % glucose. Complexes were prepared by mixing the solutions 1:1 to produce the desired N/P ratio. Polyplexes were stirred at 25 °C for 30 min to allow formation. For size and zeta-potential studies, polyplexes were prepared with calf thymus DNA and with fLuc encoding pDNA for gel electrophoresis. For *in vitro* transfection studies, stock solutions of the polymers were prepared at a concentration of 5 mg/mL in HEPES butter (20 mM, pH 7.4) and 5 wt % glucose. The polymer solution was added to the RNA solution at a ratio of 4:1 (v/v) to yield a final RNA concentration of 0.001 mg/mL such that 100 ng was added to each well of a 96-well plate.

Particle Size and Zeta-Potential Analysis. The polyplex size and zeta-potential analysis were prepared using a previously reported procedure[16] at N/P ratios of 0.5, 1, 2, 5, 10, 20, and 50 with the polymer fixed at 0.1 mg mL^{-1}. The calf thymus DNA concentration varied for each N/P ratio. Size measurements were performed directly with the prepared polyplex solutions. For zeta-potential measurements, polyplex solutions were diluted 1:1 with 10 mM NaCl (aq). Measurements were performed as described in Instrumentation and Analysis. For hydrolysis studies, polyplexes were measured at 24 h intervals and stored at 37 °C between measurements.

Gel Electrophoresis. Gel electrophoresis experiments were performed following a reported protocol.[16] Briefly, polyplexes for the gel retardation assay were prepared with a fixed DNA concentration of 200 ng mL^{-1} with polymer concentrations varied for each N/P ratio. Then, 20 μL of polyplex and 4 μL of loading dye (-SDS, 6×) were loaded onto a 1% agarose gel + GelRed in Tris-acetate-EDTA 1× (TAE) buffer, subjected to electrophoresis for 40 min at 100 V, and visualized with an UV illuminator.

In Vitro Studies. Hemolysis. Defibrinated sheep blood (7.5 mL) was centrifuged at 4500 *g* for 10 min at room temperature to collect erythrocytes. The supernatant and pellet were separated, and the supernatant was replaced with 5 mL of fresh phosphate-buffered saline (PBS) and the pellet resuspended. This was repeated until the supernatant was completely colorless. Then, the suspension was diluted 10-fold in PBS. Polyplexes were prepared with polymers P1−P8 and PEI at N/P ratios of 0.5, 5, and 50 in the HEPES buffer (0.02 M) with calf thymus DNA (0.1 mg mL^{-1}). Then, 20 μL of each polyplex was then diluted with 380 μL of erythrocyte resuspension in 1.5 mL Eppendorf tubes such that the final concentration of DNA was

50 μg mL^{-1}, 5 μg mL^{-1}, and 0.5 μg mL^{-1}. The controls of PBS and HEPES (negative) and a 1% Triton-X (positive) PBS solution were also prepared and treated as above. Erythrocyte polyplex mixtures were then incubated at 37 °C for 3 h and subsequently separated by centrifugation at 4500 *g* for 5 min. Then, 200 μL of the supernatant from each tube was removed and transferred to a clear 96-well plate, and the absorbance was read at 540 nm using a TECAN SPARK multimode plate reader. The average PBS negative control value was subtracted from nanoparticle values and divided by the average Triton-X positive control value to obtain the % hemolysis. Errors were determined using the standard deviation of the three replicates.

Cytotoxicity Assay. Cells were transfected with polyplexes prepared with luciferase encoding self-amplifying RNA (saRNA) and P1−P8 at N/P ratios of 2, 10, and 50. Then, at 24 h post-treatment, each well was treated with 20 μL of CellTiterBlue reagent (Promega, UK) and subsequently incubated for 1 h. The absorbance of each well was determined using a FLUOstar Omega plate reader (BMG LABTECH, UK) and normalized to the untreated control.

In Vitro Transfection of saRNA Polyplexes. In vitro transfection experiments were performed using a previously reported procedure.[16] Briefly, transfections were performed in HEK293T.17 cells (ATCC, USA) that were maintained in culture in complete Dulbecco's Modified Eagle's medium (cDMEM) (Gibco, ThermoFisher, UK) containing 10% (v/v) fetal calf serum (FCS), 5 mg mL^{-1} L-glutamine, and 5 mg mL^{-1} penicillin and streptomycin (ThermoFisher, UK). Cells were plated at a density of 50000 cells/well in a 96-well plate 24 h prior to transfection. At the time of transfection, the media was completely removed and replaced by 50 μL of transfection media (DMEM with 5 mg mL^{-1} L-glutamine). Then, 100 μL of the polyplex solution was added to each well and incubated for 4 h. Then, the media was replaced with cDMEM, and the cells were allowed to culture for 24 h, at which time 50 μL of media was removed, and 50 μL of the ONE-Glo D-luciferin substrate (Promega, UK) was added and mixed well by pipetting. The total volume was transferred to a white 96-well plate (Costar, UK) and analyzed on a FLUOstar Omega plate reader (BMG LABTECH, UK).

Ex Vivo Studies. Flow Cytometry Analysis of eGFP Expression in Human Skin Explants. The transfection of cells in human skin explants and the flow cytometry analysis were performed as previously described.[16] Surgically resected specimens of human skin tissue were collected at Charing Cross Hospital, Imperial NHS Trust, London, UK. All tissues were collected after receiving signed informed consent from patients, under protocols approved by the Local Research Ethics Committee (MED_RS_11_014). The tissue was obtained from patients undergoing elective abdominoplasty or mastectomy surgeries and was processed as previously described.[37] Upon arrival in the laboratory, the subcutaneous layer of fat was removed, and the tissue was excised into 1 cm^2 pieces. Explants were incubated at 37 °C with 5% CO_2 in 12-well plates with cDMEM, which was replaced daily. Explants were injected intradermally (ID) using a micro-fine Demi 0.3 mL syringe (Becton Dickinson, UK) with 5 μg of eGFP saRNA polyplexes. After 72 h, explants were digested into single cell suspensions by incubating in 2 mL of DMEM supplemented with 1 mg/mL collagenase P (Sigma, UK) and 5 mg/mL Dispase II (Sigma, UK) for 4 h at 37 °C on a rotational shaker. Digests were then filtered through a 70 μm cell strainer and centrifuged at 1750 rpm for 5 min. Cells were then resuspended in FACS buffer (PBS + 2.5% FCS) and stained with a Fixable Aqua Live/Dead Cell stain (ThermoFisher, UK) diluted at 1:400 in FACS buffer for 20 min. Cells were then washed and stained with a panel of antibodies to identify each cell type for 30 min. The antibody panel included CD3-V450 (BioLegend, UK), CD14-Qdot605 (BioLegend, UK), CD19-BV650 (BioLegend, UK), CD56-BV711 (BioLegend, UK), CD1a-PerCP-eFluor710 (BioLegend, UK), CD11c-PE (BioLegend, UK), CD90-PE-Cy7 (BioLegend, UK), and CD45-AF700 (BioLegend, UK). Cells were then fixed in 1.5% paraformaldehyde and refrigerated until the flow cytometry analysis was conducted. Samples were analyzed on a LSRFortessa (BD Biosciences, UK) with FACSDiva software (BD Biosciences, UK) with 100000 acquired cell events. Gating and

Scheme 1. Schematic Representation for RAFT Polymerization and Monomer Composition of Homopolymers and Copolymers P1−P8[a]
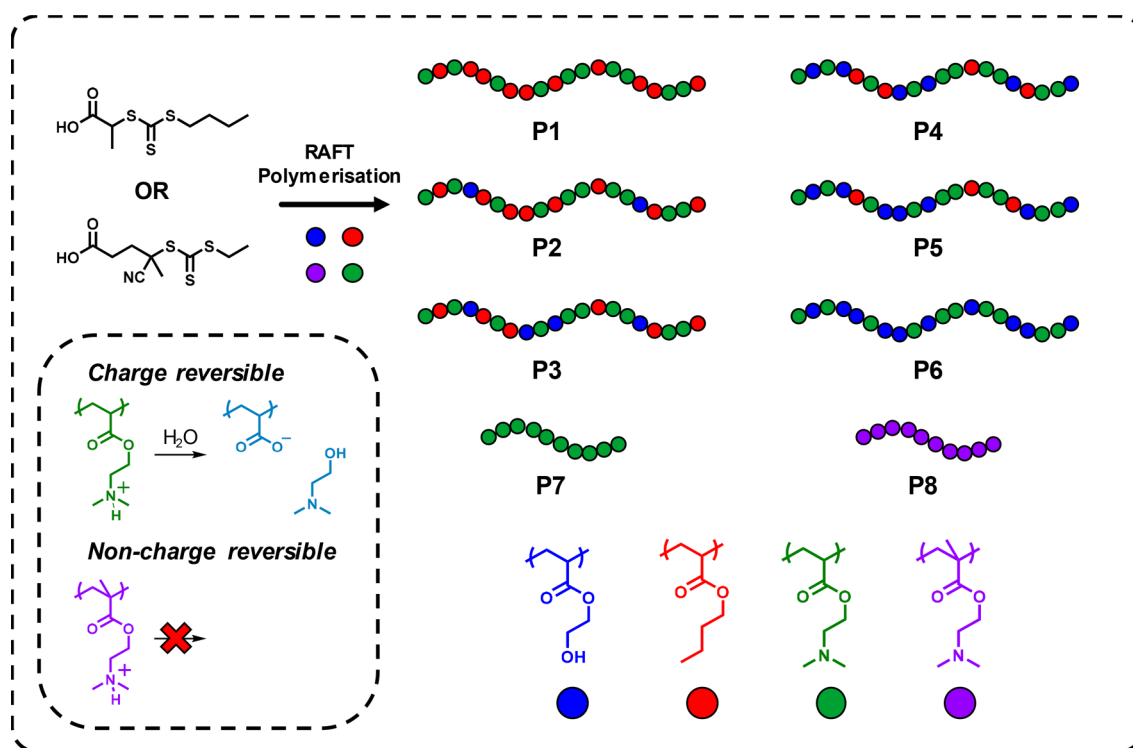
[a]Inset shows the charge reversal process.

Table 1. Structure and Characterization of the Polymers (P1−P8) Synthesized in This Study

polymer	structure	$M_{n,th}$ (g mol^{-1})[a]	$M_{n,SEC}$ (g mol^{-1})[b]	$Đ$[b]
P1	pDMAEA$_{25}$-co-BA$_{25}$	7000	3300	1.16
P2	pDMAEA$_{25}$-co-BA$_{20}$-co-HEA$_5$	6950	5400	1.22
P3	pDMAEA$_{25}$-co-BA$_{15}$-co-HEA$_{10}$	6900	7000	1.18
P4	pDMAEA$_{25}$-co-BA$_{10}$-co-HEA$_{15}$	6850	7300	1.21
P5	pDMAEA$_{25}$-co-BA$_5$-co-HEA$_{20}$	6800	7800	1.24
P6	pDMAEA$_{25}$-co-HEA$_{25}$	6700	10300	1.15
P7	pDMAEA$_{25}$	3800	3100	1.21
P8	pDMAEMA$_{25}$	4300	5000	1.22

[a]Calculated using eq 1. [b]Determined using DMF-SEC.

analysis was performed in FlowJo Version 10 (FlowJo LLC, Oregon, USA).

In Vivo Studies. In Vivo fLuc Expression. In vivo fLuc saRNA transfection experiments were performed as previously described.[19] All animals were handled in accordance with the UK Home Office Animals Scientific Procedures Act 1986 and with an internal ethics board and UK government approved project (P63FE629C) and personal license (IC37CBB8F). Food and water were supplied ad libitum. Female BALB/c mice (Charles River, UK) 6−8 weeks of age were placed into groups (n = 5) and housed in a fully acclimatized room. In vivo imaging was performed as previously described. Mice were injected either intramuscularly in both hind legs or intradermally with 5 μg of fLuc saRNA complexed with P1−P8 or PEI in a total volume of 50 μL. After 7 days, the mice were injected intraperitoneally (IP) with 100 μL of XenoLight RediJect D-luciferin substrate (PerkinElmer, UK) and allowed to rest for 10 min. Mice were then anesthetized using isoflurane and imaged on an *In Vivo Imaging System* (IVIS) FX Pro (Kodak Co., Rochester, NY, USA) equipped with Molecular Imaging software version 5.0 (Carestream Health, USA) for 2 min. The signal from each injection site was quantified using Molecular Imaging software and expressed as relative light units (p/s).

Statistical Analysis. Plots and statistics were performed using GraphPad Prism, version 8. Significant differences were identified using either multiple t tests adjusted for multiple comparisons or one-way ANOVA with multiple comparisons.

■ RESULTS AND DISCUSSION

Polymer Synthesis and Characterization. A library of eight cationic polymers (P1−P8) were synthesized using RAFT polymerization. Six (P1−P6) of these were prepared with 50 mol % charge-reversible monomer DMAEA, while the lipophilicity of the other 50 mol % was varied by increasing and decreasing (in 10 mol % increments) the quantity of HEA and BA, respectively (Scheme 1), with a total DP$_{target}$ = 50. Furthermore, pDMAEA$_{25}$ (P7) and pDMAEMA$_{25}$ (P8) homopolymers were prepared as fully hydrolyzing and nonhydrolyzing controls respectively, with the same cationic content (25 units) as P1−P6. Acrylate polymerizations were performed with the RAFT agent PABTC at 70 °C using thermal initiation with ACVA, while methacrylate polymerizations performed with RAFT agent CPAETC at 90 °C with
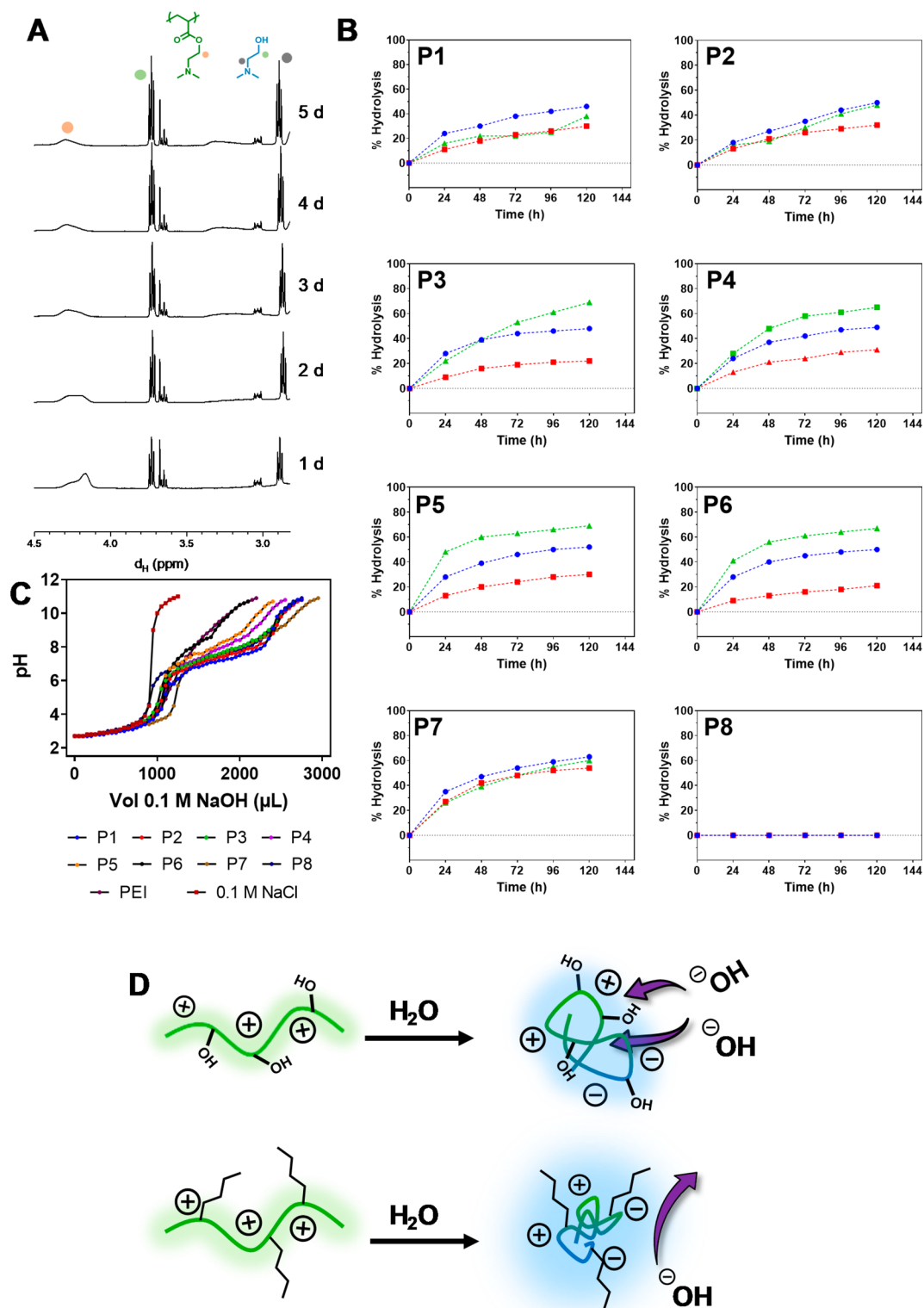
Figure 1. (A) Representative ^{1}H NMR spectrum illustrating the release of DMAE from pDMAEA homopolymer P7 over 5 days. (B) Hydrolysis kinetics derived from ^{1}H NMR spectra of P1−P8 over 5 days in D$_2$O at pH 5.5 (red line), 7.4 (blue line), and 10.1 (green line). (C) pH titration of P1−8, PEI, and 0.1 M NaCl from pH 3 to pH 11, titrated with 0.1 M NaOH (aq). (D) Schematic representation of the partial hydrolysis of pDMAEA copolymers containing either hydrophilic or hydrophobic co-monomers, leading to pH-dependent hydrolysis, due to the hydroxide access for more hydrophilic pDMAEA analogues.

VA-088. Full conditions can be found in the Supporting Information (Table S1). ^{1}H NMR spectroscopy revealed the synthesized polymers had the targeted co-monomer composi-

tion, while DMF-SEC analysis revealed narrow ($Đ < 1.25$) and monomodal chromatograms (Table 1, Figure S1, Figure S2). Some deviation between experimental and theoretical molar
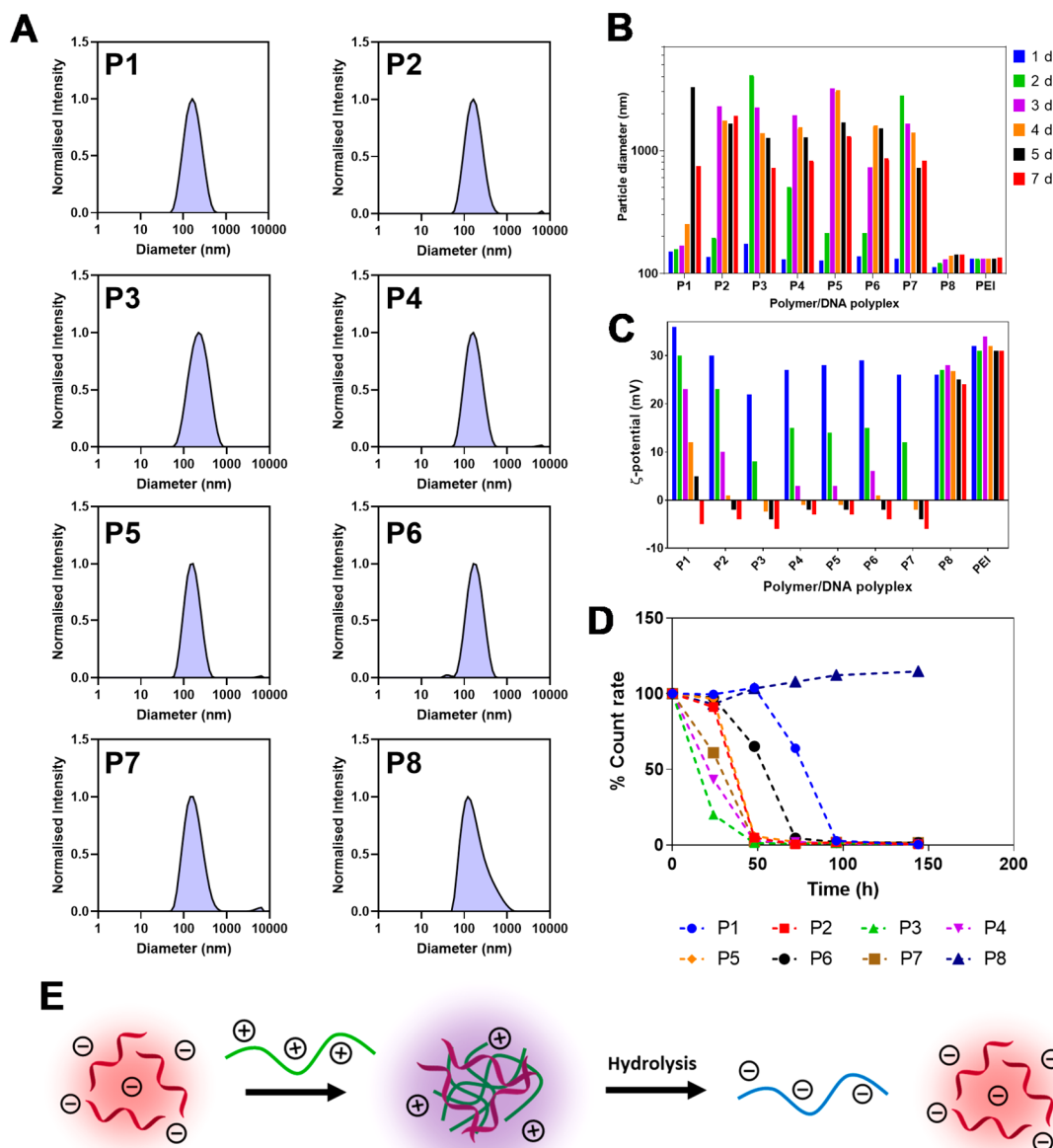
Figure 2. (A) DLS traces of polyplexes comprising P1−P8 (0.1 mg mL^{-1}) and calf thymus DNA at N/P = 10 measured at 37 °C. Evolution of (B) particle size and (C) zeta-potential of polyplexes comprising P1−P8 (0.1 mg mL^{-1}) and calf thymus DNA at N/P = 10 measured at 37 °C measured after 24 (blue), 48 (green), 72 (purple), 96 (orange), 120 (black), and 168 h (red). (D) Evolution of the derived scattering intensity/count rate of polyplexes, normalized to the initial measurement at $t = 0$ h, comprising P1−P8 (0.1 mg mL^{-1}) and calf thymus DNA at N/P = 10 measured at 37 °C over 7 days. (E) Schematic representation of nucleic acid binding, charge reversal, and subsequent nucleic acid release.

masses was observed, this was more apparent for copolymers with higher HEA mol % likely due to their greater swelling during SEC analysis. The statistical monomer distribution of DMAEA, BA, and HEA ternary copolymers was confirmed through a kinetic polymerization study performed on a mixture containing 33% of each monomer. ^{1}H NMR spectra of samples withdrawn periodically through the polymerization revealed identical polymerization kinetics for each co-monomer (Figure S3), suggesting identical reactivity ratios.

Chain Lipophilicity Induces pH Dependency on Charge Reversal. Previous reports studying the charge reversal of pDMAEA into pAA have identified a pH-independent self-catalyzed hydrolysis mechanism. However, most of these studies utilize block copolymers,[32] homopolymers,[24,25,28,31] or statistical copolymers containing co-

monomers with complementary functionalities such that there is limited spacing between basic residues within the chain.[29] Given this, we were interested in identifying if the relative lipophilicity of the copolymers impacted the rate of pDMAEA hydrolysis and its pH-independent mechanism. Hydrolysis kinetics of DMAEA side chains in P1−P8 was determined by recording daily ^{1}H NMR spectra at pH 5.5, 7.4, and 10.1, monitoring the reduction and increase of integrals of the signals at 4.2 ppm (CH$_2$ next to ester in polymer) and 3.7 ppm (CH$_2$ next to alcohol in DMAE), respectively (Figure 1A and Figure S4). Where copolymers were sparingly soluble at the beginning of the study, a soluble external reference of 1,3,5-trioxane was added to the NMR tubes, and the integrals were back-calculated at the end of the study, at which point

deuterium chloride was added to protonate and solubilize the copolymers to quantify the percentage hydrolysis.

P1−P6 exhibited comparable hydrolysis rates, reaching ∼50 and 20−30% hydrolysis at pH 7.4 and 5.5 respectively, over 5 days at 37 °C. In contrast, at pH 10.1 the more hydrophobic copolymers (P1 and P2) hydrolyzed significantly slower rates (∼40% over 5 days) than the more hydrophilic derivatives (∼60% over 5 days), with the kinetic profiles revealing a trend of faster hydrolysis with increasing hydrophilicity (Figure 1B). We hypothesize that the slower hydrolysis in P1 and P2 at pH 10.1 may be due to the DMAEA residues being deprotonated at pH 10.1, causing these analogues to be sparingly soluble in the early stages of hydrolysis. However, once a significant portion is hydrolyzed, the resulting acrylic acid residues are deprotonated at this pH, improving the solubility, which may explain the increased hydrolysis rate observed after 72 h. Consistent with the literature, the pDMAEA homopolymer P7 showed almost identical hydrolysis rates at all three pH values, reaching 60% over the course of the experiment, while the nonhydrolyzing pDMAEMA homopolymer P8 did not show any significant signs of hydrolysis.

Interestingly, we observed that the difference in the hydrolysis rate and the final percentage of hydrolysis between pH 5.5 and pH 10.1 increased significantly with the hydrophilic co-monomer composition. For instance, after 5 days, P1 reached 30, 37, and 45% hydrolysis at pH 5.5, 7.4, and 10.2, respectively, which represented a 15% difference between acidic and basic conditions. In contrast, P6 was hydrolyzed to extents of 20, 50, and 65%, a difference of 45% under the same treatment conditions (Figure 1B). While DMAEA homopolymers typically exhibit pH-independent hydrolysis, here we demonstrate a pH-dependent hydrolysis controlled by the hydrophobicity of the co-monomer. We anticipate this behavior may originate depending on the solubility of the zwitterionic complex, which is formed as hydrolysis approaches 50%. In this state, the chains will be partially positive and partially negative, collapsing due to the intramolecular electrostatic attraction. The more hydrophobic derivatives will be less prone to charge reversal due to the poor hydration of these collapsed chains, slowing their hydrolysis (Figure 1D). This behavior may be important in gene delivery, leading to the potential of a pH-dependent controlled release of nucleic acids, or in anatomies and cellular compartments with nonphysiological pH levels.

Lipophilic Polyplexes Charge Invert Slower than Hydrophilic Derivatives. Prior to formulating the synthesized polymers with nucleic acids, we investigated the buffering capacity of P1−P8 by titrating dilute polymer solutions with 0.1 M NaOH from pH 2.5 to pH 11. P1−P7 displayed similar titration curves, with two observable pK_a values, one at ∼ pH 5 and the other at ∼ pH 10. These were compared to PEI, the reference standard in gene transfection, and P8, the pDMAEMA homopolymer (Figure 1C). Both showed poorer buffering with less defined pK_a values, likely due to the density of basic residues minimizing the propensity of these analogues for successive protonation events.

Polyplex formulations were optimized using model nucleic acids, either with calf thymus DNA or luciferase-encoding plasmid DNA. Particle size, zeta-potential measurements, and gel-retardation assays were performed on polyplexes at N/P ratios of 0.5, 1, 2, 5, 10, 20, and 50. Stable complexes, displaying narrow particle size distributions (PDi < 0.3), positive zeta-potentials above 20 mV, and full DNA-binding

abilities were observed above N/P = 5 (Figure S5). All polymers yielded polyplexes of similar sizes, exhibiting average diameters between 120 to 200 nm (Figure 2A). The particle size (Figure 2B) and zeta-potentials (Figure 2C) of polyplexes formulated at N/P = 10 utilizing the charge-reversible polymers (P1−P7) evolved steadily over 1 week as hydrolysis progressed. Interestingly, instead of decreasing in size as polymers in polyplexes hydrolyzed, the polyplex diameters increased from ∼150 nm to over 1000 nm (Figure 2B). However, at this time point, the scattering intensity of the solutions rapidly decreases (Figure 2D), indicating partial or full disassembly of the polyplex, but the increase in particle size, visible via DLS (Figure 2B), is likely due to a few aggregated particles when the zeta potentials reach ∼0 mV, skewing the light scattering analysis. The charge-reversible nature of P1−P7 was evidenced by the steadily decreasing zeta-potentials, decreasing from positive (∼30 mV) to negative (−6 mV) as the cationic DMAEA units hydrolyzed to anionic acrylic acid residues (Figure 2C). The nonhydrolyzing pDMAEMA homopolymer P8 exhibited some aggregation, increasing from 110 to 145 nm diameters between 1 and 7 days, while the zeta-potentials showed minimal change (Figure 2B). The zeta-potentials and scattering intensity of the hydrophobic copolymers decreased significantly slower than hydrophilic analogues, likely due to the lower hydration potential of these complexes, slowing the self-catalyzed hydrolysis process. These results indicate that polyplexes formulated with self-hydrolyzing analogues should be effective at releasing nucleic acids, and the particles themselves will dissociate, potentially avoiding bioaccumulation.

Hydrophobic Polyplexes Are the Most Cytotoxic yet Induce the Highest Protein Expression *In Vitro*. We assessed the membrane interactions of polyplexes derived from our library of polymers by evaluating their propensity to lyse erythrocytes (hemolysis, Figure 3A). Polyplexes derived from P1−P8 and PEI were formulated at N/P = 0.5, 5, and 50. Their hemolytic activity was compared to Triton-X (positive control), HEPES buffer (vehicle control), free DNA and PBS (negative control). The observable increasing trend in hemolytic activity with increasing N/P ratios is likely due to the higher concentration of free polymer not residing in the polyplex. Previous studies have indicated that, although the nominal N/P ratio in the solution typically exceeds 10, the *actual* N/P ratio within the complex usually does not exceed 2; thus, substantially more free polymer is present at high N/P ratios.[38,39] At N/P = 50, a stepwise increase in the hemolytic activity was observable with more hydrophobic analogues, starting with negligible hemolysis in P6 polyplexes and rising to 97% hemolysis, which is almost identical to the positive control, in P1 polyplexes (Figure 3A). It is well documented that polycations incorporating hydrophobic residues are exceptionally membrane active due to their attraction to the phospholipid bilayer and disruptive hydrophobic interactions. The hemolytic activity has also been a key marker for high endosomal escape efficiencies and thus may give insight into the mechanisms of RNA delivery for these polymers.[40]

Following this, the *in vitro* transfection efficiency and cytotoxicity of polyplexes comprising fLuc-encoding saRNA and polymers P1−P8 at N/P ratios of 2, 10, and 50 in HEK293T cells after 24 h of incubation were also assessed (Figure 3B). From a vaccination perspective, saRNA poses significant advantages over conventional mRNA, as these constructs self-replicate upon their arrival in the cytoplasm,
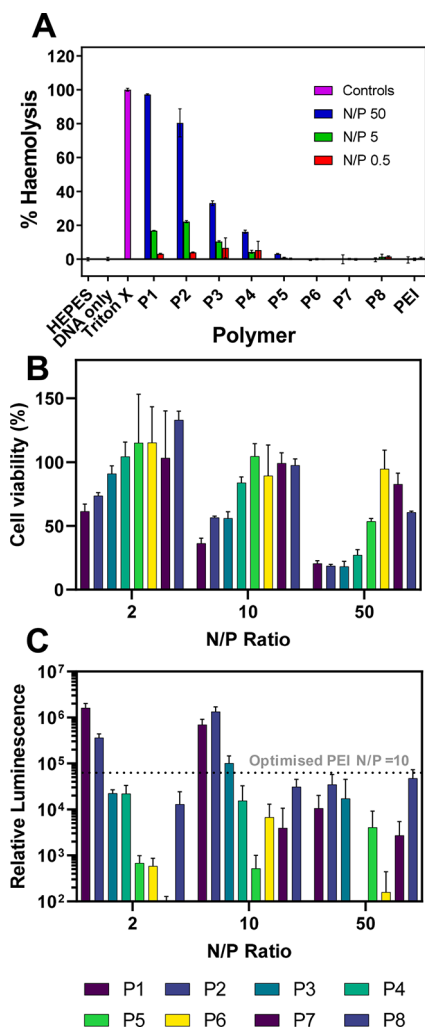
Figure 3. (A) Hemolytic activity of calf thymus DNA polyplexes comprising P1−8 and PEI at N/P ratios of 50, 5, and 0.5, measured after 3 h of incubation with erythrocytes collected from defibrinated sheep blood. Cell viability as a function of (B) metabolic activity and (C) luciferase expression in HEK 293T cells 24 h after transfection with polyplexes formed of P1−P8 and fLuc saRNA compared to a previously optimized PEI formulation (dotted gray line). Data are represented as the mean ± standard deviation ($n = 3$).

substantially reducing the required dose for effective immunization. The saRNA complexes displayed particle sizes similar to those prepared with model DNA for the hydrolysis studies above. However, saRNA polyplexes exhibited more negative zeta potentials than DNA analogues, potentially attributed to the poorer condensation of the larger nucleic acid with relatively low molar mass polycations (Figure S6). This is consistent with a previous report indicating complexes with high molar mass polycations at high N/P ratios display positive zeta potentials, while low molar mass analogues showed negative potentials.[19] As in the case of the hemolytic activity, the polyplexes derived from all of the synthesized polymers at higher N/P ratios were significantly more cytotoxic, again likely due to the higher concentration of noncomplexed polymer. Interestingly, P6 and P7, the most hydrophilic derivatives, and the pDMAEA homopolymer were the least cytotoxic at any N/P ratio (Figure 3B). We anticipate that the absence of BA units and the faster hydrolysis may account for the higher compatibility, which would negate any membrane

damaging properties. Analogues with more BA units displayed significantly higher cytotoxicities (P1 > P2 > P3 > P4), likely arising from stronger membrane disruption at all three N/P ratios,[41] in accordance with the hemolytic activity data.

Using the same fLuc reporter saRNA polyplexes at N/P ratios of 2, 10 and 50, *in vitro* transfection was assessed in HEK293T cells after 24 h of incubation, comparing these to an optimized PEI formulation (N/P = 10) as a positive control (Figure 3C). The more hydrophilic analogues P3−P6 displayed similar or lower transfection efficiencies than PEI ($\sim 6.5 \times 10^4$ RLU) at all three N/P ratios. Remarkably, P1 and P2, the copolymers containing the highest BA composition, exhibited significantly higher transfection efficiencies than PEI at N/P = 2 ($\sim$24-fold and $\sim$5.5-fold higher for P1 and P2, respectively) and N/P = 10 ($\sim$11-fold and $\sim$20-fold for P1 and P2, respectively, Figure 3A). Coupled to the previous cytotoxicity data, the lower transfection efficiencies at higher N/P ratios are likely a product of the reduced number of cells available for transfection. Nonetheless, the lower cell viabilities for P1 and P2 at N/P = 2 and N/P = 10 indicate an even higher transfection efficiency per cell compared to the hydrophilic derivatives P3−P6, with only $\sim$60% of viable cells still producing up to 24-fold higher luciferase in this cell population compared to PEI formulations.

Hydrophobic Polyplexes Enhance the Number of saRNA-Expressing Cells in Human Skin Explants. For RNA vaccines to be easily incorporated into current clinical practices, it has been posited that these would be administered through traditional intramuscular or intradermal injections.[42] We therefore examined the transfection efficiency of a subset of the formulations tested *in vitro* in an *ex vivo* human skin explant model (Figure 4A). Polymers P1, P3, P6, P7, and P8 were formulated into polyplexes with saRNA encoding for green fluorescent protein (GFP) at N/P = 10. Nonformulated RNA yielded expression in $\sim$2% of cells, which did not significantly increase upon complexation with P3 ($p = 0.92$), P6 ($p > 0.99$), P7 ($p = 0.94$), and P8 ($p = 0.99$). However, formulations with P1, the most effective polymer *in vitro*, showed a significant increase in GFP$^+$ cells ($\sim$11%) compared to RNA alone ($p = 0.022$, Figure 4A). The numbers of GFP+ cells in these studies were similar to those in previous studies with mannosylated PEI-saRNA complexes[43] but were higher than those with cationic lipid-saRNA formulations.[37]

Although many of the formulations did not increase the percentage of GFP$^+$ cells, skin is a complex tissue comprising many cell types in their native tissue architecture. We therefore sought to identify *which* cells were expressing the GFP. Transfected skin explants were enzymatically homogenized, and each cell type was labeled using a panel of fluorescently labeled antibodies. Then, GFP$^+$ cells were categorized by cell type via flow cytometry (Figure 4B). We observed that the cell phenotype in the skin used was predominantly epithelial ($\sim$60%), with leukocytes ($\sim$8%) and fibroblasts ($\sim$11%), and dendritic ($\sim$10%) with a much smaller proportion of Langerhans cells ($\sim$0.8%), natural killer (NK) cells ($\sim$1%), monocytes ($\sim$3%), B cells ($\sim$4%), and T cells ($\sim$0.5%). In skin treated with nonformulated RNA, the majority of GFP expression was found in the commonly found epithelial cells, leukocytes, and fibroblasts; however, some enrichment was observed in NK cells, B cells, and Langerhans cells compared to the cell composition of the skin (Figure 4B). The profile of GFP$^+$ cells was generally similar for skin treated with polyplexes derived from the faster hydrolyzing hydrophilic
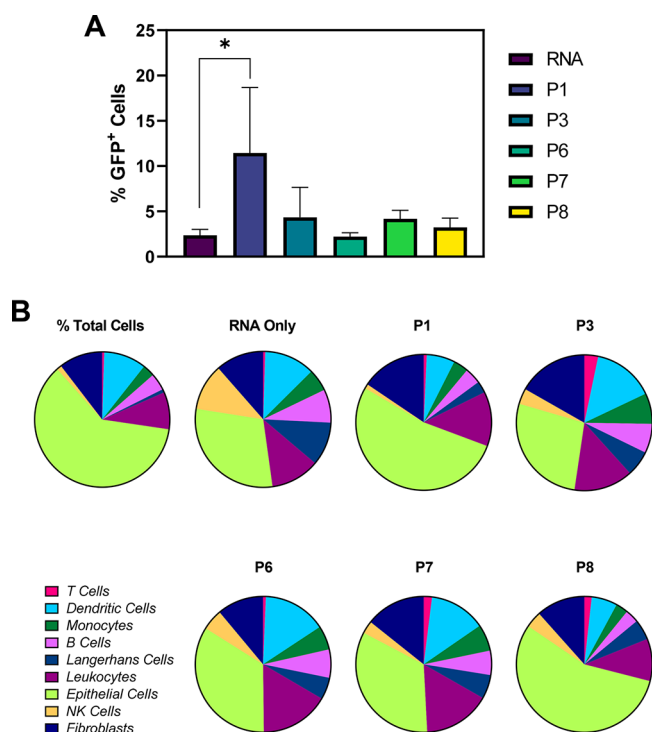
Figure 4. (A) Proportion of GFP-positive cells from the total of live cells in human skin explants. Data are represented as the mean ± standard deviation (n = 3). Asterisks indicate relevant statistically significant results (*$p \leq 0.05$, **$p \leq 0.01$, ***$p \leq 0.001$). (B) Cell-type profile in human skin explants and GFP+ cells after the injection of polymer-saRNA formulations, as determined by flow cytometry.
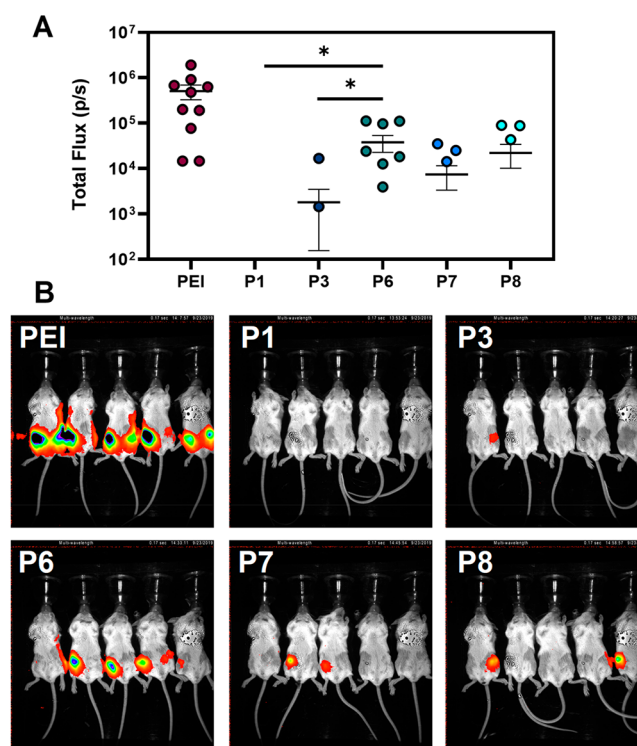

Figure 5. (A) Quantitation of *in vivo* fLuc expression 7 days after IM injection of PEI, P1, P3, P6, P7, and P8 saRNA (5 μg) polyplexes at N/P = 10. Each circle represents one leg of one animal, and the bar represents the mean ± SEM, n = 5. Asterisks indicate relevant statistically significant results (*$p \leq 0.05$, **$p \leq 0.01$, and ***$p \leq 0.001$). Note that P1, P3, P6, P7, and P8 are all significantly different to PEI (***). (B) Images of each group 7 days after IM injection of fLuc saRNA polyplexes.

derivatives (P3, P6, and P7), with some enrichment in the immune cell population. In contrast, skin treated with P1 and P8, which both show slow or negligible charge reversal, had similar expression profiles with a significantly higher expression in epithelial cells, closely matching the resident skin cell population (Figure 4B). From these observations, we can conclude that P1 polyplexes at N/P = 10 enhance the number of GFP+ cells in human skin explants due to an increase in the expression from epithelial cells.

***In Vivo* Studies.** Following the successful transfection of 2D cell monolayers and human skin explants mediated by our charge-reversing polymers, we sought to evaluate their potential in saRNA vaccination using an *in vivo* murine model. Mice were injected intramuscularly on each leg with polyplexes composed of charge-reversing polymers P1, P3, P6, P7, and P8 with fLuc-encoding saRNA at N/P = 10. These polymers were chosen such that we could examine the trends in polymer hydrophobicity (P1, P3, and P6) and the effect of charge reversal (P7 and P8) with a minimal number of animals. The selected polymers were formulated for saRNA complexation at N/P = 10 for consistency with *in vitro* and *ex vivo* skin studies. The luminescence was monitored 7 days after injection at the expected time point for peak expression (Figure 5A and B). Charge-reversible formulations were compared to the pDMAEMA nonhydrolyzing control P8 and an *in vivo* optimized PEI formulation (jetPEI). In contrast to the data obtained in the *in vitro* and *ex vivo* experiments, in the murine model, the PEI formulation outperformed all polyplexes, yielding an average luminescence of ∼5.0 × 10⁵ RLU. Mice administered with P1, P3, P6, P7, and P8 had a rather variable luminescence, with no groups exhibiting RNA expression on

every injected leg. In contrast again to the *in vitro* and *ex vivo* results above, P1 yielded no RNA expression across all five animals, while mice treated with P6 polyplexes exhibited 7/10 positive legs with an average luminescence of ∼4 × 10⁴, roughly 10-fold lower than that of PEI (Figure 5A and B). It is possible that the poor translation of P1 for *in vitro* to *in vivo* protein expression arose due to the previously observed toxic membrane interactions, causing local cell death proximal to the injection site, or to local self-association/aggregation of the more hydrophobic complexes in the protein-rich muscle regions, of which both factors would have reduced transfection. In contrast, polyplexes derived from P6, P7, and P8, which were the least cytotoxic or membrane active, yielded the highest efficacy *in vivo*, which may have been a consequence of the high vascularization in muscle and rapid transport of polyplexes following injection. In addition, animals treated with the charge-reversible pDMAEA homopolymer (P7) displayed similar luminescence values to those injected with the nonhydrolyzing pDMAEMA control (P8). These data perhaps indicate that the unpackaging of RNA from the polyelectrolyte complexes is not the rate-limiting step in transfection and expression of the target protein *in vivo*, at least for these types of polymers injected into this anatomical site (Figure 5A and B). There is always a trade-off between the tight-binding of nucleic acids to afford colloidal stability in a formulation and protection against nucleases following injection and the ability to enter target cells and address the translational machinery. In a site of high blood vessel and

protein content, such as a site following intramuscular injection, the polyplexes have the potential to bind to many other biomolecules prior to reaching a target cell. In addition, the processing of RNA *in vivo* involves multiple competitive binding interactions intracellularly, and these may have been sufficient to the unpackaging of RNA from the complexes, irrespective of whether the side-chains in the polycations were hydrolyzing.

Finally, it should be noted that the polymers in this study were designed as probes of transfection rather than materials to be adopted in the clinic, as the acrylate-based chain is not biodegradable. Nevertheless, as they are chemically well-defined, the polymers could be used to test systematically the effects of side-chain hydrophilicity and hydrophobicity in conjunction with side-chain hydrolysis and charge-reversal in a manner not possible for main-chain biodegradable polymers. Our future studies will focus on further probing the mechanisms by which the RNA polyplexes are transported and unpackaged in as close to clinically relevant *in vivo* models as possible.

CONCLUSIONS

In conclusion, we designed a systematic library of charge-reversible polymeric gene delivery vectors, varying the relative lipophilicity of copolymers based on the self-catalyzed hydrolysis of pDMAEA. By spacing DMAEA units with hydrophobic units, we were able to produce self-hydrolyzing polymers with pH-dependent hydrolysis. In contrast, hydrophilic residues diminished the pH dependency. Although there was a negligible effect of polymer hydrophobicity on the charge reversal at physiological pH levels, once formulated with nucleic acids, the more hydrophobic derivatives exhibited slower charge reversal, which is attributed to the reduced hydration of the complex. Although all polymers displayed similar buffering and nucleic acid binding capacities, the stronger membrane activity of hydrophobic analogues likely led to a 10- to 20-fold increase in the *in vitro* transfection efficiency over PEI albeit with significant cytotoxicity. Similarly, the most hydrophobic derivative P1 yielded a higher percentage of transfected cells in human skin explants, ascribed to transfection enrichment in epithelial cells. The superior performance of the hydrophobic analogues, however, did not translate *in vivo*, as they were outcompeted by the hydrophilic derivatives. In general, we observed limited benefit *in vitro* or *in vivo* with charge-reversible vectors (comparing pDMAEA and pDMAEMA homopolymers), but these factors may be more important from a toxicity and pharmacokinetic perspective. This study clearly indicates the importance of lipophilicity of nonviral vectors. We anticipate the results found here will help direct future nonviral gene delivery vector design, with a particular focus on RNA vaccines given the relevant data in human skin and *in vivo* models.

ASSOCIATED CONTENT

Supporting Information

The Supporting Information is available free of charge at https://pubs.acs.org/doi/10.1021/acs.biomac.0c00698.

> Supporting Information contains detailed information on the polymerization conditions and characterization data for the synthesized polymers, ^{1}H NMR spectra for hydrolysis studies, and physical characterization of polyplexes (PDF)

AUTHOR INFORMATION

Corresponding Authors

Cameron Alexander − *Division of Molecular Therapeutics and Formulation, School of Pharmacy, University of Nottingham, Nottingham NG7 2RD, United Kindom;* orcid.org/0000-0001-8337-1875; Email: cameron.alexander@nottingham.ac.uk

Robin J. Shattock − *Department of Infectious Disease, Imperial College London, School of Medicine, St Mary's Hospital, London W2 1NY, United Kindom;* Email: r.shattock@imperial.ac.uk

Authors

Pratik Gurnani − *Division of Molecular Therapeutics and Formulation, School of Pharmacy, University of Nottingham, Nottingham NG7 2RD, United Kindom;* orcid.org/0000-0002-6559-5514

Anna K. Blakney − *Department of Infectious Disease, Imperial College London, School of Medicine, St Mary's Hospital, London W2 1NY, United Kindom;* orcid.org/0000-0002-5812-9689

Roberto Terracciano − *Division of Molecular Therapeutics and Formulation, School of Pharmacy, University of Nottingham, Nottingham NG7 2RD, United Kindom; Drug Delivery Laboratory, Department of Pharmacy, University of Napoli Federico II, 80131 Napoli, Italy*

Joshua E. Petch − *Division of Molecular Therapeutics and Formulation, School of Pharmacy, University of Nottingham, Nottingham NG7 2RD, United Kindom*

Andrew J. Blok − *Division of Molecular Therapeutics and Formulation, School of Pharmacy, University of Nottingham, Nottingham NG7 2RD, United Kindom*

Clément R. Bouton − *Department of Infectious Disease, Imperial College London, School of Medicine, St Mary's Hospital, London W2 1NY, United Kindom*

Paul F. McKay − *Department of Infectious Disease, Imperial College London, School of Medicine, St Mary's Hospital, London W2 1NY, United Kindom;* orcid.org/0000-0001-5195-6254

Complete contact information is available at:
https://pubs.acs.org/10.1021/acs.biomac.0c00698

Notes

The authors declare no competing financial interest.

■ REFERENCES

(1) Sahin, U.; Karikó, K.; Türeci, Ö. mRNA-based therapeutics — developing a new class of drugs. *Nat. Rev. Drug Discovery* **2014**, *13* (10), 759−780.

(2) Pardi, N.; Hogan, M. J.; Porter, F. W.; Weissman, D. mRNA vaccines — a new era in vaccinology. *Nat. Rev. Drug Discovery* **2018**, *17* (4), 261−279.

(3) Guan, S.; Rosenecker, J. Nanotechnologies in delivery of mRNA therapeutics using nonviral vector-based delivery systems. *Gene Ther.* **2017**, *24* (3), 133−143.

(4) Kauffman, K. J.; Webber, M. J.; Anderson, D. G. Materials for non-viral intracellular delivery of messenger RNA therapeutics. *J. Controlled Release* **2016**, *240*, 227−234.

(5) Thess, A.; Grund, S.; Mui, B. L.; Hope, M. J.; Baumhof, P.; Fotin-Mleczek, M.; Schlake, T. Sequence-engineered mRNA Without Chemical Nucleoside Modifications Enables an Effective Protein Therapy in Large Animals. *Mol. Ther.* **2015**, *23* (9), 1456−1464.

(6) Doener, F.; Hong, H. S.; Meyer, I.; Tadjalli-Mehr, K.; Daehling, A.; Heidenreich, R.; Koch, S. D.; Fotin-Mleczek, M.; Gnad-Vogt, U. RNA-based adjuvant CV8102 enhances the immunogenicity of a licensed rabies vaccine in a first-in-human trial. *Vaccine* **2019**, *37* (13), 1819−1826.

(7) Alberer, M.; Gnad-Vogt, U.; Hong, H. S.; Mehr, K. T.; Backert, L.; Finak, G.; Gottardo, R.; Bica, M. A.; Garofano, A.; Koch, S. D.; Fotin-Mleczek, M.; Hoerr, I.; Clemens, R.; von Sonnenburg, F. Safety and immunogenicity of a mRNA rabies vaccine in healthy adults: an open-label, non-randomised, prospective, first-in-human phase 1 clinical trial. *Lancet* **2017**, *390* (10101), 1511−1520.

(8) Gan, L.-M.; Lagerström-Fermér, M.; Carlsson, L. G.; Arfvidsson, C.; Egnell, A.-C.; Rudvik, A.; Kjaer, M.; Collén, A.; Thompson, J. D.; Joyal, J.; Chialda, L.; Koernicke, T.; Fuhr, R.; Chien, K. R.; Fritsche-Danielson, R. Intradermal delivery of modified mRNA encoding VEGF-A in patients with type 2 diabetes. *Nat. Commun.* **2019**, *10* (1), 871.

(9) Kis, Z.; Shattock, R.; Shah, N.; Kontoravdi, C. Emerging Technologies for Low-Cost, Rapid Vaccine Manufacture. *Biotechnol. J.* **2018**, *14* (1), 1800376.

(10) Kis, Z.; Papathanasiou, M.; Calvo-Serrano, R.; Kontoravdi, C.; Shah, N. A model-based quantification of the impact of new manufacturing technologies on developing country vaccine supply chain performance: A Kenyan case study. *J. Adv. Manuf. Process.* **2019**, *1* (3), e10025.

(11) Kowalski, P. S.; Rudra, A.; Miao, L.; Anderson, D. G. Delivering the Messenger: Advances in Technologies for Therapeutic mRNA Delivery. *Mol. Ther.* **2019**, *27* (4), 710−728.

(12) Blakney, A. K.; McKay, P. F.; Christensen, D.; Yus, B. I.; Aldon, Y.; Follmann, F.; Shattock, R. J. Effects of cationic adjuvant formulation particle type, fluidity and immunomodulators on delivery and immunogenicity of saRNA. *J. Controlled Release* **2019**, *304*, 65−74.

(13) Blakney, A. K.; McKay, P. F.; Yus, B. I.; Aldon, Y.; Shattock, R. J. Inside out: optimization of lipid nanoparticle formulations for exterior complexation and in vivo delivery of saRNA. *Gene Ther.* **2019**, *26* (9), 363−372.

(14) Démoulins, T.; Milona, P.; Englezou, P. C.; Ebensen, T.; Schulze, K.; Suter, R.; Pichon, C.; Midoux, P.; Guzmán, C. A.; Ruggli, N.; McCullough, K. C. Polyethylenimine-based polyplex delivery of self-replicating RNA vaccines. *Nanomedicine* **2016**, *12* (3), 711−722.

(15) Vogel, A. B.; Lambert, L.; Kinnear, E.; Busse, D.; Erbar, S.; Reuter, K. C.; Wicke, L.; Perkovic, M.; Beissert, T.; Haas, H.; Reece, S. T.; Sahin, U.; Tregoning, J. S. Self-Amplifying RNA Vaccines Give Equivalent Protection against Influenza to mRNA Vaccines but at Much Lower Doses. *Mol. Ther.* **2018**, *26* (2), 446−455.

(16) Saviano, F.; Lovato, T.; Russo, A.; Russo, G.; Bouton, C. R.; Shattock, R. J.; Alexander, C.; Quaglia, F.; Blakney, A. K.; Gurnani, P.; Conte, C. Ornithine-derived oligomers and dendrimers for in vitro delivery of DNA and ex vivo transfection of skin cells via saRNA. *J. Mater. Chem. B* **2020**, *8* (22), 4940−4949.

(17) Cook, A. B.; Peltier, R.; Zhang, J.; Gurnani, P.; Tanaka, J.; Burns, J. A.; Dallmann, R.; Hartlieb, M.; Perrier, S. Hyperbranched poly(ethylenimine-co-oxazoline) by thiol−yne chemistry for non-viral gene delivery: investigating the role of polymer architecture. *Polym. Chem.* **2019**, *10* (10), 1202−1212.

(18) Blakney, A. K.; Abdouni, Y.; Yilmaz, G.; Liu, R.; McKay, P. F.; Bouton, C. R.; Shattock, R. J.; Becer, C. R. Mannosylated Poly(ethylene imine) Copolymers Enhance saRNA Uptake and Expression in Human Skin Explants. *Biomacromolecules* **2020**, *21* (6), 2482−2492.

(19) Blakney, A. K.; Zhu, Y.; McKay, P. F.; Bouton, C. R.; Yeow, J.; Tang, J.; Hu, K.; Samnuan, K.; Grigsby, C. L.; Shattock, R. J.; Stevens, M. M. Big Is Beautiful: Enhanced saRNA Delivery and Immunogenicity by a Higher Molecular Weight, Bioreducible, Cationic Polymer. *ACS Nano* **2020**, *14* (5), 5711−5727.

(20) Ganta, S.; Devalapally, H.; Shahiwala, A.; Amiji, M. A review of stimuli-responsive nanocarriers for drug and gene delivery. *J. Controlled Release* **2008**, *126* (3), 187−204.

(21) Hu, Y.; Gong, X.; Zhang, J.; Chen, F.; Fu, C.; Li, P.; Zou, L.; Zhao, G. Activated Charge-Reversal Polymeric Nano-System: The Promising Strategy in Drug Delivery for Cancer Therapy. *Polymers* **2016**, *8* (4), 99.

(22) McKinlay, C. J.; Vargas, J. R.; Blake, T. R.; Hardy, J. W.; Kanada, M.; Contag, C. H.; Wender, P. A.; Waymouth, R. M. Charge-altering releasable transporters (CARTs) for the delivery and release of mRNA in living animals. *Proc. Natl. Acad. Sci. U. S. A.* **2017**, *114* (4), E448−E456.

(23) Feng, C.; Shen, Z.; Li, Y.; Gu, L.; Zhang, Y.; Lu, G.; Huang, X. PNIPAM- b -(PEA- g -PDMAEA) double-hydrophilic graft copolymer: Synthesis and its application for preparation of gold nanoparticles in aqueous media. *J. Polym. Sci., Part A: Polym. Chem.* **2009**, *47* (7), 1811−1824.

(24) Truong, N. P.; Jia, Z.; Burges, M.; McMillan, N. A. J.; Monteiro, M. J. Self-Catalyzed Degradation of Linear Cationic Poly(2-dimethylaminoethyl acrylate) in Water. *Biomacromolecules* **2011**, *12* (5), 1876−1882.

(25) Truong, N. P.; Jia, Z.; Burgess, M.; Payne, L.; McMillan, N. A. J.; Monteiro, M. J. Self-Catalyzed Degradable Cationic Polymer for Release of DNA. *Biomacromolecules* **2011**, *12* (10), 3540−3548.

(26) Cotanda, P.; Wright, D. B.; Tyler, M.; O'Reilly, R. K. A comparative study of the stimuli-responsive properties of DMAEA and DMAEMA containing polymers. *J. Polym. Sci., Part A: Polym. Chem.* **2013**, *51* (16), 3333−3338.

(27) Sun, F.; Feng, C.; Liu, H.; Huang, X. PHEA- g -PDMAEA well-defined graft copolymers: SET-LRP synthesis, self-catalyzed hydrolysis, and quaternization. *Polym. Chem.* **2016**, *7* (45), 6973−6979.

(28) Whitfield, R.; Anastasaki, A.; Truong, N. P.; Wilson, P.; Kempe, K.; Burns, J. A.; Davis, T. P.; Haddleton, D. M. Well-Defined PDMAEA Stars via Cu(0)-Mediated Reversible Deactivation Radical Polymerization. *Macromolecules* **2016**, *49* (23), 8914−8924.

(29) Cook, A. B.; Peltier, R.; Hartlieb, M.; Whitfield, R.; Moriceau, G.; Burns, J. A.; Haddleton, D. M.; Perrier, S. Cationic and hydrolysable branched polymers by RAFT for complexation and controlled release of dsRNA. *Polym. Chem.* **2018**, *9* (29), 4025−4035.

(30) Chroni, A.; Pispas, S. Hydrophilic/hydrophobic modifications of a PnBA-b-PDMAEA copolymer and complexation behaviour with short DNA. *Eur. Polym. J.* **2020**, *129*, 109636.

(31) Liao, X.; Falcon, N. D.; Mohammed, A. A.; Paterson, Y. Z.; Mayes, A. G.; Guest, D. J.; Saeed, A. Synthesis and Formulation of Four-Arm PolyDMAEA-siRNA Polyplex for Transient Downregulation of Collagen Type III Gene Expression in TGF-β1 Stimulated Tenocyte Culture. *ACS Omega* **2020**, *5* (3), 1496−1505.

(32) Truong, N. P.; Gu, W.; Prasadam, I.; Jia, Z.; Crawford, R.; Xiao, Y.; Monteiro, M. J. An influenza virus-inspired polymer system for the timed release of siRNA. *Nat. Commun.* **2013**, *4* (1), 1902.

(33) Ros, S.; Kleinberger, R. M.; Burke, N. A. D.; Rossi, N. A. A.; Stöver, H. D. H. Charge-Shifting Polycations with Tunable Rates of Hydrolysis: Effect of Backbone Substituents on Poly[2-

(dimethylamino)ethyl acrylates]. *Macromolecules* **2018**, *51* (15), 5752−5761.

(34) Ros, S.; Wang, J.; Burke, N. A. D.; Stöver, H. D. H. A Mechanistic Study of the Hydrolysis of Poly[N, N -(dimethylamino)-ethyl acrylates] as Charge-Shifting Polycations. *Macromolecules* **2020**, *53* (9), 3514−3523.

(35) Gurnani, P.; Lunn, A. M.; Perrier, S. Synthesis of mannosylated and PEGylated nanoparticles via RAFT emulsion polymerisation, and investigation of particle-lectin aggregation using turbidimetric and DLS techniques. *Polymer* **2016**, *106*, 229−237.

(36) Larnaudie, S. C.; Brendel, J. C.; Jolliffe, K. A.; Perrier, S. Cyclic peptide−polymer conjugates: Grafting-to vs grafting-from. *J. Polym. Sci., Part A: Polym. Chem.* **2016**, *54* (7), 1003−1011.

(37) Blakney, A. K.; McKay, P. F.; Ibarzo Yus, B.; Hunter, J. E.; Dex, E. A.; Shattock, R. J. The Skin You Are In: Design-of-Experiments Optimization of Lipid Nanoparticle Self-Amplifying RNA Formulations in Human Skin Explants. *ACS Nano* **2019**, *13* (5), 5920−5930.

(38) Ma, P.; Buschmann, M. D.; Winnik, F. M. Complete physicochemical characterization of DNA/chitosan complexes by multiple detection using asymmetrical flow field-flow fractionation. *Anal. Chem.* **2010**, *82* (23), 9636−43.

(39) Ma, P. L.; Buschmann, M. D.; Winnik, F. o. M. One-Step Analysis of DNA/Chitosan Complexes by Field-Flow Fractionation Reveals Particle Size and Free Chitosan Content. *Biomacromolecules* **2010**, *11* (3), 549−554.

(40) Evans, B. C.; Nelson, C. E.; Yu, S. S.; Beavers, K. R.; Kim, A. J.; Li, H.; Nelson, H. M.; Giorgio, T. D.; Duvall, C. L. Ex vivo red blood cell hemolysis assay for the evaluation of pH-responsive endo-somolytic agents for cytosolic delivery of biomacromolecular drugs. *J. Visualized Exp.* **2013**, No. 73, e50166−e50166.

(41) Kuroda, K.; Caputo, G. A.; DeGrado, W. F. The Role of Hydrophobicity in the Antimicrobial and Hemolytic Activities of Polymethacrylate Derivatives. *Chem. - Eur. J.* **2009**, *15* (5), 1123−1133.

(42) Zhang, C.; Maruggi, G.; Shan, H.; Li, J. Advances in mRNA Vaccines for Infectious Diseases. *Front. Immunol.* **2019**, *10*, 594.

(43) Blakney, A. K.; Abdouni, Y.; Yilmaz, G.; Liu, R.; McKay, P. F.; Bouton, C. R.; Shattock, R. J.; Becer, C. R. Mannosylated Poly(ethylene imine) Copolymers Enhance saRNA Uptake and Expression in Human Skin Explants. *Biomacromolecules* **2020**, *21* (6), 2482−2492.